Relaxation time of dilute polymer solutions: A microfluidic approach

Francesco Del Giudice, Simon J. Haward, and Amy Q. Shen

Citation: Journal of Rheology **61**, 327 (2017);
View online: https://doi.org/10.1122/1.4975933
View Table of Contents: http://sor.scitation.org/toc/jor/61/2
Published by the The Society of Rheology

Relaxation time of dilute polymer solutions: A microfluidic approach

Francesco Del Giudice,[a] Simon J. Haward, and Amy Q. Shen

Micro/Bio/Nanofluidics Unit, Okinawa Institute of Science and Technology Graduate University, Okinawa, Japan

(Received 22 November 2016; final revision received 18 January 2017; published 15 February 2017)

Abstract

Polymer solutions are considered *dilute* when polymer chains in a solution do not interact with each other. One important step in the characterization of these systems is the measurement of their longest relaxation times λ. For dilute polymer solutions in low-viscous solvents, this measurement can be very challenging through conventional techniques. Recently, several microfluidic platforms have been successfully employed to measure the rheological properties of weakly viscoelastic solutions. Nevertheless, a comparison between data generated from different microfluidic platforms has not yet been presented. In this work, we measure λ of dilute polymer solutions for concentrations down to a few parts per million, by using two distinct microfluidic platforms with shear and extensional flow configurations. We consider three representative polymer classes: Neutral polymers in near-theta and good solvents, and a biological polyelectrolyte in a good solvent in the presence of salt. Relaxation times in shear flow λ_{shear} are measured through the μ-rheometer based on the viscoelastic alignment of particles in a straight microchannel. Relaxation times in extensional flow λ_{ext} are measured in a microfluidic optimized cross-slot configuration based on the onset of the flow-induced birefringence. A good agreement between experimental measurements from the two platforms is found. Experimental measures are also compared with available theories. © *2017 The Society of Rheology*.
[http://dx.doi.org/10.1122/1.4975933]

I. INTRODUCTION

Dilute polymer solutions have attracted tremendous interest from both fundamental and applied perspectives for almost a century [1–4]. Some of the first thermodynamic studies on dilute polymer solutions were conducted by Alfrey and Doty [1] in 1945, later extended by the work of Rouse [2] and Zimm [3]. These works focused on the response of a single macromolecule when subjected to hydrodynamic forces. Dilute polymer solutions are also important in many industrial applications such as drag reduction in pipe flows, stabilization of jets [5], and in the development of household cleaning products [6,7].

More recently, dilute polymer solutions have found new exciting applications with the advent of microfluidics [8]. Polymer solutions have been used for particle alignment and separation [9], and dilute polymer solutions are often preferred over concentrated solutions because of their relatively low viscosity, thus avoiding pumping problems [10]. Dilute polymer solutions have also displayed interesting flow phenomena in both shear and extensional microfluidics. For example, when flowing in a serpentine microchannel, elastic instability in a curved geometry was observed (in analogy with the elastic instability in Couette flow) [11–13]. Moreover, the elastic instability was found to depend on the rheological parameters of the polymer solution. Dilute polymer solutions were also investigated in various extensional microfluidic devices with cross-slot and expansion-contraction geometries [14–20].

Dilute polymer solutions are characterized by several rheological parameters, among which the viscosity and the relaxation time assume great importance [21]. The viscosity is a measure of the drag exerted by the fluid as a response to an external flow field, and is relatively easy to measure through a conventional bulk rheometry or by microfluidic slit rheometry [22,23]. The relaxation time λ is related to the amount of elastic energy being stored by the fluid. Polymer solutions can possess a spectrum of relaxation times, related to a relaxation process occurring within and outside the chain itself [24]. For polymer melts above the entanglement molecular weight, the existence of multiple relaxation times is related to the strong interactions of polymer chains with other surrounding polymer chains (i.e., reptation) [21]. On the other hand, there are no interactions between polymer chains in ideal dilute solutions of isolated macromolecules. Neutral chains (those without free charges) adopt a random coil configuration in dilute solution [24]. Thus, the relaxation time spectrum in a dilute polymer solution has contributions from the multiple relaxation processes occurring on the single subchains, and those related to the entire chain. If the dilute polymer system renders a monodisperse molecular weight distribution, we can assume that all chains relax simultaneously from a uniformly deformed state with the *longest* time scale possible, because the relaxation time of the entire chain is slower than that of the subchains. In this scenario, the viscoelasticity of a dilute polymer solution can be quantified by its longest relaxation time.

Unfortunately, the determination of the relaxation time λ for dilute polymer solutions is generally challenging, particularly in shear flows, because of the low viscoelasticity of the solution (λ-values on the order of tens of milliseconds and below, in low-viscous solvents such as water) [25,26].

[a]Author to whom correspondence should be addressed; electronic mail: francesco.delgiudice@me.com

Conventional shear rheological techniques do not offer a satisfying solution, because of the detection limit of the instrumentation caused by the onset of inertial effects [25,26]. In this context, microfluidics has emerged as a promising tool for capturing the rheological properties of fluids, and in particular the fluid relaxation time in shear flow, which are otherwise not detectable through conventional bulk rheometry [23,25–27]. The first of the kind was the serpentine *microrheometer* of Zilz *et al.* [25], where shear relaxation time on the order of 1 ms for dilute aqueous polyethylene oxide (PEO) solutions has been reported. Zilz *et al.* [11] also reported that PEO solutions from different batches (at the same polymer concentration and molecular weight) exhibited different relaxation times. Thus, PEO may not be the best choice of the polymer sample to use for the comparison (especially interlaboratory comparison) of different relaxation time measurement techniques. More recently, Del Giudice *et al.* [26] introduced a novel microfluidic platform, the μ-rheometer, based on the transverse migration of particles suspended in viscoelastic fluids flowing in a straight microchannel. This platform was very recently employed for the study of polyelectrolytes in glycerol-water solutions (25% of glycerol) [28], in both salt-free and salt-rich conditions, in the dilute regime. In particular, values of the shear relaxation time down to 60 μs were measured. We remark that existing studies on the measurement of the shear relaxation time through microfluidic techniques deal mainly with aqueous based solutions.

In contrast, extensional flow based techniques to measure the relaxation time of dilute polymer solutions have been more successful [20,29,30,32,33]. Opposed-jet and cross-slot extensional flow devices, in fact, have been used to measure relaxation times below 1 ms since the 1980s [20]. More recently, a number of capillary-thinning based measurement techniques have been proposed. Campo-Deaño and Clasen [30] reported a variation of the conventional Capillary Breakup Extensional Rheometer (CaBER). They monitored the filament breakup by using a high-speed camera, being able to measure relaxation times down to 240 μs. Vadillo *et al.* [31] monitored the filament stretching of polystyrene dissolved in diethyl phthalate with a high-speed camera. They were able to detect relaxation times as small as 80 μs. Bhattacharjee *et al.* [35] used surface acoustic waves to generate the viscoelastic filament as in the CaBER, but achieved a much higher sensitivity compared with the classical CaBER. Keshavarz *et al.* [32] reported a microfluidic technique based on the Rayleigh Ohnesorge Jetting Extensional Rheometer (ROJER), capable of measuring relaxation times down to 60 μs. Dinic *et al.* [33] measured relaxation times below 1 ms by observing the capillary thinning and pinch-off dynamics of aqueous polymer solutions, generated by dripping the liquid directly onto a substrate. Sousa *et al.* [34] studied the capillary thinning breakup of dilute polymer solutions in an immiscible oil bath (minimizing the fluid evaporation), and measured relaxation times down to 100 μs. Very recently, Haward [20] conducted a comprehensive review on microfluidic extensional rheometry using stagnation point flow (e.g., flow in a crossslot configuration), by employing the onset of the flow-induced birefringence in an extensional microfluidic device to extract the relaxation time of polymer solutions (see Sec. III D 1 for more details).

The abundance of measurement platforms inspired us to make comparisons between the experimental values derived through different shear and extensional microfluidic techniques on well-known polymer solutions (such as polystyrene solutions in organic solvents). To the best of our knowledge, such studies are not available in the literature.

In this work, we compare the fluid relaxation time λ of dilute polymer solutions measured in both microfluidic shear and extensional flows, for three distinctive polymer classes. We carried out experiments on polystyrene in both near-theta and good solvents, and on high molecular weight hyaluronic acid (i.e., a biological polyelectrolyte) in a good solvent with the presence of salt. To measure the relaxation time λ_{shear} in a shear flow, we adopted the μ-rheometer of Del Giudice *et al.* [26,28], based on the viscoelastic alignment of particles in a straight microchannel. To measure the relaxation time in an extensional flow λ_{ext}, we use an extensional microfluidic platform based on the onset of flow induced birefringence in an optimized cross-slot device [19], hereafter referred as the "OSCER." Our results show that (i) relaxation time down to a few ms can be measured with both microfluidic platforms. (ii) For neutral polymers in near-theta and good solvents, $\lambda_{ext} \simeq \lambda_{shear}$, both depending on the polymer concentration with a scaling that is consistent with the Rouse theory [2]. (iii) For hyaluronic acid in a good solvent with the presence of salt, only λ_{shear} can be determined because the low birefringence of the material under investigation prohibits measures in the OSCER device. (iv) For the polymer in near-theta solvent and polyelectrolyte in good solvents, the constant relaxation time derived from our experiments is in quantitative agreement with the Zimm formula [see Eq. (2)] [3].

II. THEORETICAL BACKGROUND

Before presenting our results, it is important to give a brief background on the behavior of polymers in solutions. When a polymer chain is added to a solvent, various thermodynamic interactions take place [24]. The polymer chains in solution usually adopt a coil-like configuration. The dimension of the coil depends on the competition between two intramolecular interactions: The steric repulsion between monomers and the solvent-mediated attraction between monomers [24]. The θ temperature is the state at which these two intramolecular interactions are perfectly balanced (do not confuse with the dimensionless parameter Θ in Sec. III C 1). The solvent for the polymer at the θ temperature is called theta (or θ) solvent. A solvent is called good when the temperature $T > \theta$, thus the steric repulsion prevails over the solvent-mediated attraction *(excluded volume)*, and then the coil swells, being bigger than that in a θ solvent. A common way to characterize the quality of a solvent for a given polymer at a certain temperature is based on the evaluation of the *dimensionless scaling exponent* ν. This parameter is related to the volume occupied by the random-coil in solution, with

$\nu = 0.5$ for polymers in a theta-solvent and $\nu = 0.6$ for polymers in a good solvent [24].

Different conformations of the polymer in solution, i.e., more or less swelled, lead to different scalings of macroscopic properties such as viscosity and relaxation time, with respect to the polymer concentration c. When the polymer concentration is well below the so-called overlapping concentration c^* (the concentration at which polymer chains start to interact), macroscopic properties are expected to be well described by the Zimm model [3]. The scaling laws predicted for the specific zero-shear viscosity $\eta_{sp0} = (\eta_0 - \eta_s)/\eta_s$, where η_0 is the zero-shear viscosity, η_s is the solvent viscosity, and the relaxation time λ in the dilute regime are

$$\eta_{sp0} \propto c \quad \text{and} \quad \lambda \propto c^0. \tag{1}$$

Note that λ is independent of the polymer concentration when $c < c^*$. The relaxation time in the dilute regime can also be evaluated through the Zimm formula [3]

$$\lambda_{Zimm} = \frac{F[\eta]M_w\eta_s}{RT}, \tag{2}$$

where $F = 1/\sum_{i=1}^{N}(1/i^{3\nu})$ is a parameter depending on the solvent quality (through the dimensionless scaling exponent ν), $[\eta]$ is the intrinsic viscosity of the polymer, M_w is the molecular weight, R is the universal gas constant, and T is the absolute temperature.

When increasing the polymer concentration c in the vicinity of c^*, polymer coils start to interact, thus hydrodynamic interactions are screened by the presence of other polymer chains [2,24]. In this case, the theoretical predictions are derived from the Rouse theory [2], and the scaling laws are

$$\eta_{sp0} \propto c^{1/(3\nu-1)} \quad \text{and} \quad \lambda \propto c^{(2-3\nu)/(3\nu-1)}. \tag{3}$$

In this regime, polymer chains interact without forming entanglements. At higher concentrations, polymer chains entangle, and the prediction becomes different from that of Eq. (3).

For polyelectrolyte solutions, scalings are much more complex, and depend on many more parameters such as the number of monomers in the electrostatic blob or the number of monomers between uncondensed charges [36]. In this work, we deal with polyelectrolytes in a good solvent and in the presence of large amount of salt, i.e., in the so-called *high-salt limit*. In this case, scalings are identical [37] to those for uncharged polymer in a good solvent [Eqs. (1)–(3) with $\nu = 0.6$], because electrostatic interactions between the charges on the polyelectrolyte are analogous to the excluded volume [38,39].

III. MATERIALS AND METHODS

A. Materials

We select three representative dilute polymer systems for the relaxation time measurements. The first two systems involve a neutral polymer, atactic polystyrene (a-PS, Agilent technologies, USA), suspended in two different solvents with varying solvent quality: A poor solvent at near-theta conditions and a good solvent. The third system involves a polyelectrolyte, hyaluronic acid (HA, Sigma Aldrich, USA) in water solution with the presence of salt.

For the a-PS polymer system, a-PS with average molecular weight $M_w = 6.9$ MDa (Agilent, USA) and molecular weight dispersity $M_w/M_n = 1.09$ (where M_w and M_n are the mass and numeric molecular weight, respectively) at mass concentrations ranging from 0.008 wt. % to 0.14 wt. %, is suspended in either dioctyl phthalate (DOP), a theta solvent at 22 °C [40,41], or in tricresyl phosphate (TCP), a good solvent at room temperature [42]. Fluids are prepared by diluting a stock solution of a-PS in the given solvent to the required test concentration. Stock solutions are prepared by dissolving a weighed quantity of polystyrene into 50 ml of dichloromethane for 24 h. This solution was then dissolved into either DOP or TCP in a glass bottle, and mixed for four weeks on a hot plate ($T = 30$ °C) with a magnetic stirrer in order to remove the dichloromethane. A filter paper was placed over the neck of the glass bottle in order to allow evaporation of the dichloromethane while preventing external contamination of the fluid sample. The mass of the mixing sample was measured daily to track the evaporation of the dichlorometane. The mass of the sample was found to be stable after four weeks.

For the HA polymer system, HA with average molecular weight $M_w = 1.6$ MDa at mass concentrations ranging from 0.0005 wt. % to 0.08 wt. % are dissolved in the phosphate-buffered saline (PBS, Sigma Aldrich, Japan), and in water at different salt concentrations (sodium chloride, NaCl). PBS contains mainly 138 mM of NaCl and 2.7 mM of KCl, and is a widely used physiological buffer for biological samples [37,43]. The molecular weight dispersity of HA samples similar to that used here is typically reported to be within the range $1.1 < M_w/M_n < 1.2$ [47,48,54]. The solution was stirred continuously for 2 days to reach sample uniformity. Solutions with 50 mM of NaCl and 100 mM of NaCl were also prepared by following the same procedure described previously. Lower polymer concentrations were prepared by dilution.

Microbeads are added to each polymer solution to measure λ_{shear} in the μ-rheometer. Specific particle diameters are selected to keep the confinement ratio $\beta = D_p/H \sim 0.1$, where D_p is the particle diameter and H is the channel width. Poly(methyl methacrylate) particles in dry powder form (Microparticles GmbH) with an average diameter of 8 μm are suspended directly in DOP and TCP. Polystyrene particles (PS, Polysciences) with an average diameter $D_p = 10\,\mu$m or $D_p = 6\,\mu$m are suspended in the HA solutions. The final mass concentration of particles in each solution is maintained at $\phi = 0.01$ wt. %.

B. Bulk shear rheometry

For bulk shear rheometry, all polymer solutions were characterized by a steady-shear flow procedure using a stress controlled shear rheometer (Anton Paar MCR 502). The temperature was fixed at 22 °C. Evaporation of aqueous samples

was controlled by using a solvent trap, and shear rates were varied from 10^{-1} to $10^{3}\,s^{-1}$. A stainless-steel cone-plate geometry (50 mm in diameter and 1°) was used for all measurements.

C. The μ-rheometer device

1. Working principle of the μ-rheometer

The working principle of the μ-rheometer (schematic shown in Fig. 1) can be summarized as follows. Solid particles suspended in viscoelastic fluids in a straight microchannel tend to migrate transversely to the flow direction when subjected to a Poiseuille flow [26,44]. When exploring the constant-viscosity zone of a viscoelastic suspending liquid, Romeo *et al*. showed that under inertialess conditions [45], suspended particles migrated toward the centerline, depending on a single dimensionless parameter

$$\Theta = De\frac{L}{H}\beta^2 = De\frac{LD_p{}^2}{H^3}, \tag{4}$$

where L is the distance from the channel inlet (see Fig. 1), H is the channel width, $\beta = D_p/H$ is the confinement ratio (with D_p being the particle diameter), and $De = k\lambda_{shear}\dot{\gamma}_c$ is the Deborah number, with λ_{shear} the shear relaxation time, and $\dot{\gamma}_c$ is the characteristic shear rate. The value of the parameter k depends on the unit of λ_{shear}, with $k = 1$ for $\lambda_{shear} = [s/rad]$ (as derived from the linear viscoelastic response with the angular frequency ω expressed in rad/s), and $k = 1/2\pi$ for $\lambda_{shear} = [s]$. In this work, we use $k = 1/2\pi$ because the value of λ_{ext} is measured in seconds.

The fraction of particles aligned on the centerline, f_1, can be described by [26]

$$f_1 = \frac{1}{1 + Be^{-C\Theta^2}}. \tag{5}$$

The above equation is an interpolating analytical expression of the theoretical model depicting the transversal migration of particles in straight channels, with constants $B = 2.7$ and $C = 2.75$ as the best curve fit constants [26]. Equation (5) is calculated based on the balance between the elastic force (which allows transversal migration) and the drag force [45]. Here, the elastic force is modeled from the second order fluid constitutive equation, with a single (longest) fluid relaxation time scaling linearly with the Deborah number De [21,45]. By measuring the fraction of particles aligned on the channel centerline (by simple optical microscopy) at a distance L from the inlet position, the parameter Θ can be easily evaluated. The relaxation time λ_{shear} can be subsequently calculated by using Eq. (4). Note that the interpolating function of Eq. (5) is only valid when $\Theta < 1$, i.e., generally for small De (values of $De \sim 0.1$–0.5 have been previously used [26,45]) and small confinement ratio $\beta \sim 0.1$, based on the underlying assumptions of the theoretical model [45]. Once these conditions are satisfied, Eq. (5) can be used as a *universal relationship*, thus no calibration is required.

In this work, we use a cylindrical microchannel, with channel diameter D, and the characteristic shear rate is $\dot{\gamma}_c = 4Q/\pi D^3$. The shear relaxation time λ_{shear} expressed in s can be derived from the inversion of Eq. (5)

$$\lambda_{shear} = 2\pi\frac{\pi}{4}\frac{1}{\beta^2}\frac{D^4}{LQ}\sqrt{\frac{1}{C}\ln\left(\frac{f_1 B}{1 - f_1}\right)}. \tag{6}$$

Note that by reducing the channel diameter D, it is possible to measure smaller values of the relaxation time λ_{shear}. More details on the theoretical background can be found in the original paper [26].

2. Experimental conditions

Straight glass cylindrical capillaries (Vitrocom, USA) were glued directly to the needle of the syringe (see Fig. 1), serving as the μ-rheometer. Capillaries with two different internal diameters ($D = 50\,\mu m$ and $D = 100\,\mu m$) were selected. Based on Eq. (6), capillaries with smaller diameters can resolve smaller relaxation times of the dilute polymer solution. Hence, the glass capillary with $D = 50\,\mu m$ is used for HA solutions with $c < 0.01$ wt. %.

The fluid is pumped through the glass capillary at an imposed volumetric flow rate Q using a high precision Harvard PHD-Ultra syringe pump. We used Hamilton Gastight glass syringes to avoid wall deformation from affecting the rate of fluid delivery into the microchannel.

The alignment of particles in the μ-rheometer is observed through an inverted microscope Leica DMIRB with a 4× objective for $D = 100\,\mu m$ and a 10× objective for $D = 50\,\mu m$. Images are captured at a location $L = 7$ cm downstream from the capillary entrance using a high speed camera (Phantom Miro M310, Vision Research), at frame rates ranging between 200 and 1000 frames per second (fps).

All the experiments in the μ-rheometer were carried out at room temperature $T = 25 \pm 1$ °C, i.e., close to the theta conditions for a-PS in DOP system.

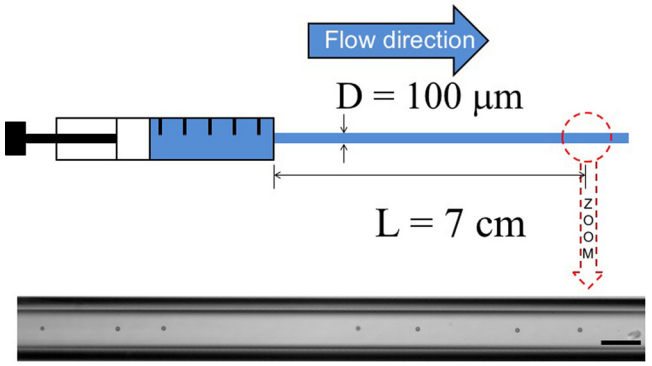

FIG. 1. Schematic of the microfluidic channel used for the measurement of the fluid relaxation time λ_{shear} in shear flow. The glass cylindrical microcapillary is glued directly to the syringe. The distance from the inlet at which the particle migration phenomenon is observed (for the measurement of λ_{shear}) is $L = 7$ cm (see Sec. III C 1 for more details). The total length of the channel is 8 cm. The scale bar represents 100 μm.

D. The OSCER device

1. Working principle of the OSCER

The extensional relaxation times λ_{ext} of the viscoelastic test fluids are measured using an Optimized Shape Cross-slot Extensional Rheometer (OSCER) [19,46], see Fig. 2(a). The measurement is based on the principle of finding the strain rate $\dot{\epsilon}$ at which the coil-stretch transition occurs [49–53]. This is determined by measuring the flow-induced birefringence at the stagnation point of the OSCER device as the strain rate is gradually incremented. The flow-induced birefringence arises due to orientation and alignment of macromolecules and is thus intimately associated with the coil-stretch transition [16,17,53]. The strain rate applied to fluid elements passing through the OSCER device is given by $\dot{\epsilon} = 0.1\ (U/(H/2))$, where $U = Q/(Hd)$ is the average flow velocity, H is the channel width, d is the channel depth, and Q is the volumetric flow rate through each inlet and outlet [19,46]. At low strain rates, the polymer remains only weakly deformed from its coil-like configuration, and the resulting birefringence is too weak to register [see Fig. 2(b)].

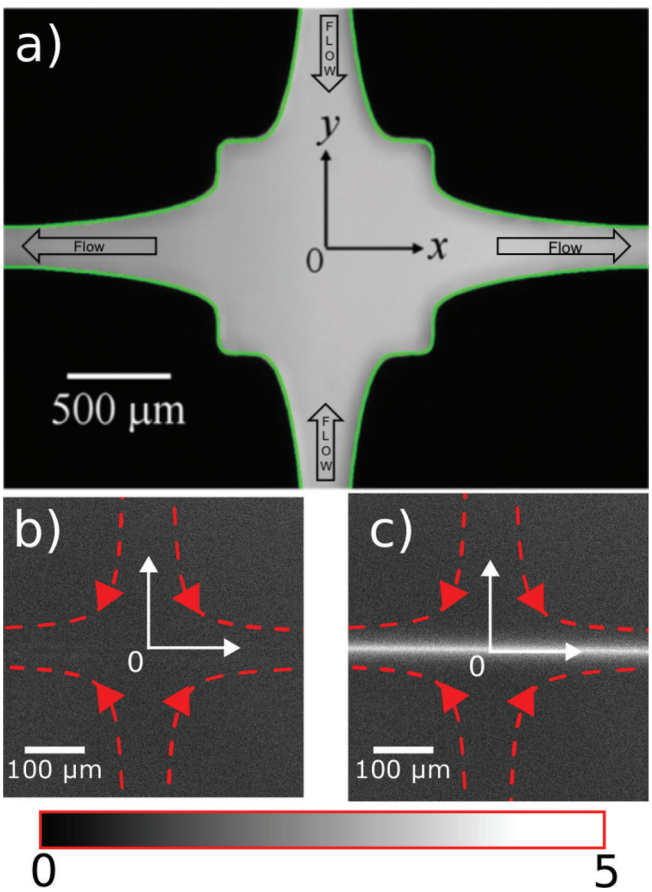

FIG. 2. (a) Experimental image of an OSCER device. Flow into the device is along the y-axis while the outflow is along the x-axis. The reference system is at the center of the geometry, in correspondence to the stagnation point. (b) and (c) Experimental images of the birefringence in the center of the OSCER device, for a 0.03% solution of a-PS in TCP. (b) At a strain rate $\dot{\epsilon} = 12.5\ s^{-1}$, no signal is observed at the stagnation point. (c) The birefringence in the center of the OSCER device, for a 0.03% solution of a-PS in TCP at a strain rate $\dot{\epsilon} = 62.5\ s^{-1}$. A clear birefringence signal is observed originating from the stagnation point. The retardance is measured in nm. Red dashed lines represent the hyperbolic flow achieved in the device.

At higher strain rates, the flow-induced birefringence appears strongly in a localized strandlike region passing through the stagnation point, thus indicating that macromolecules have undergone the coil-stretch transition [see Fig. 2(c)]. The occurrence of the coil-stretch transition is predicted when the Weissenberg number $W_i = \lambda_{ext}\dot{\epsilon}$ exceeds a critical value $W_{i_c} = \lambda_{ext}\dot{\epsilon}_c = 0.5$ [50,52,54]. By finding the critical strain rate $\dot{\epsilon}_c$ above which birefringence is observed, the relaxation time can be consequently evaluated as $\lambda_{ext} = 0.5/\dot{\epsilon}_c$. The first nonzero value of the birefringence when increasing the strain rate is considered as the onset of flow-induced birefringence, and used for the evaluation of λ_{ext}.

2. Experimental conditions

The OSCER device was fabricated via wire electrical discharge machining (EDM) in stainless steel and is fitted with glass windows to create enclosed channels with high quality optical axis to the region of interest surrounding the stagnation point. Fabrication in stainless steel and glass results in a channel with a high resistance to deformation and permits the use of organic solvents. The characteristic channel width is $H = 200\ \mu$m, while the channel depth is $d = 2100\ \mu$m. The ratio of $d/H > 10$ provides a close approximation to a 2D extensional flow field. More details on the OSCER device are available in a number of previous publications [19,20,54].

Steady flow through the OSCER device is achieved using four high precision neMESYS syringe pumps (Cetoni GmbH) fitted with Hamilton Gastight glass syringes. Two of the syringe pumps inject fluid at an equal rate into the two inlet channels, while the remaining two pumps withdraw fluid at the same rate from the two outlet channels. All the experiments in the OSCER device were carried out at room temperature $T = 25 \pm 1\ ^\circ$C, i.e., near the theta conditions for the a-PS in the DOP system.

3. Birefringence imaging

Flow-induced birefringence measurements are carried out using an Exicor Microimager birefringence imaging microscope (Hinds Instruments, Inc.). This instrument is based on a dual photoelastic modulator system and can make full-field quantitative birefringence images using a seven-frame image processing algorithm [55,56]. The seven individual images required for the birefringence determination are captured at a rate of 1 frame per second onto a 2048×2048 pixel 16-bit CCD array. The retardance resolution is 0.01 nm with a detection limit of 0.1 nm. With a $10\times$ objective lens (as used here), the field of view is approximately 1×1 mm, and the spatial resolution is approximately 0.5 μm/pixel.

IV. RESULTS AND DISCUSSION

A. Polystyrene in near-theta and good solvents

1. Bulk shear rheology

First, bulk shear rheology measurements are carried out on a-PS in DOP (near-theta solvent) and a-PS in TCP (good solvent). Figure 3(a) shows the shear viscosity η as a

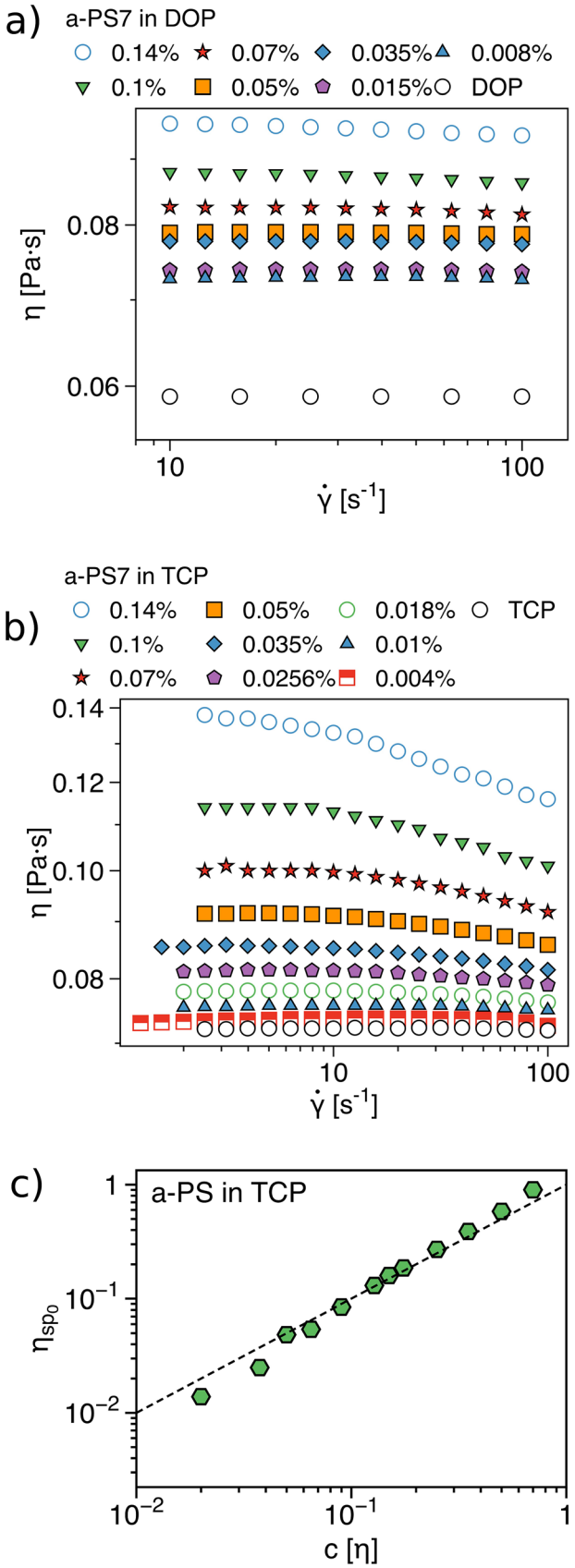

FIG. 3. (a) Shear viscosity η as a function of the shear rate $\dot{\gamma}$ for solutions at different concentrations of atactic polystyrene a-PS 7 MDa in (a) DOP (theta solvent) at 22 °C and (b) TCP at 22 °C (good solvent). (c) Specific viscosity as a function of the quantity $c[\eta]$ for a-PS 7 MDa in TCP, where $[\eta]$ is the intrinsic viscosity. The dashed line is $\eta_{sp0} = c[\eta]$.

function of the shear rate $\dot{\gamma}$, for the a-PS at concentrations from 0.008 wt. % to 0.14 wt. % in DOP. At 22 °C, DOP is a theta solvent for a-PS [40,41]. The fluid shows a constant shear viscosity in the whole range of shear rates ($10 < \dot{\gamma} < 100\,\mathrm{s}^{-1}$) for all concentrations. We can estimate the overlap concentration of a-PS in DOP as [57]

$$c^* = \frac{M_w}{N_A \frac{4}{3}\pi R g^3} \sim 0.54\%, \tag{7}$$

where M_w is the polymer molecular weight, N_A is the Avogadro number, and R_g is the radius of gyration. For the polystyrene in DOP, the value $R_g = 82\,\mathrm{nm}$ is derived from the data available in the Polymer Handbook [58]. Referring to Eq. (7), it is evident that our a-PS in DOP solutions exist in the dilute solution regime over the entire range of experimental polymer concentration.

Figure 3(b) shows the shear viscosity η as a function of the shear rate $\dot{\gamma}$ for a-PS in TCP (a good solvent for polystyrene at $T = 22\,^{\circ}\mathrm{C}$) [42]. At high a-PS concentrations, solutions show a constant value of the viscosity up to $\dot{\gamma} \sim 10\,\mathrm{s}^{-1}$, then display a slight shear-thinning response. At concentrations $c < 0.018$ wt. %, the shear-viscosity displays a near constant value in the shear rate range investigated ($1 < \dot{\gamma} < 100\,\mathrm{s}^{-1}$). To identify the overlap concentration of our polymer solutions, we consider the specific viscosity as a function of the quantity $c[\eta]$ [see Fig. 3(c)], where $[\eta]$ is the intrinsic viscosity of the polymer solution. In the dilute regime, the specific viscosity of a polymer solution at zero-shear η_{sp0} is predicted to be [59]

$$\eta_{sp0} = c[\eta], \tag{8}$$

where the intrinsic viscosity $[\eta] = 4.94\,\mathrm{dl/g}$ is evaluated from the same set of experimental data shown in Fig. 3(c). This is in good agreement with the value $[\eta] = 5.87\,\mathrm{dl/g}$ derived from the Mark-Houwink relation with parameters derived from [60]. When the experimental data deviate from the straight line $\eta_{sp,0} = c[\eta]$, the solution moves from the dilute to the semidilute regime. In Fig. 3(c), data lie on the straight line, indicating the fluids are within the dilute solution regime. The overlap concentration is estimated as $c^* = 1/[\eta] \sim 0.2$ wt. %, thus confirming that all the concentrations (0.004 to 0.14 wt. %) investigated in this study are in the dilute regime [24].

2. Microfluidic approach

We now proceed to describe the results on the fluid relaxation time of polystyrene in near-theta and good solvent conditions, derived through our μ-rheometer and the OSCER.

Figure 4(a) shows the comparison between the relaxation time of polystyrene in DOP, derived through the μ-rheometer (blue open circles) and those derived from the OSCER (green triangle). Relaxation times as small as 5 ms have been detected by both microfluidic platforms. λ_{ext} and λ_{shear} are in very good agreement when $c/c^* < 0.1$, with a small deviation observed at $c/c^* > 0.1$. Nevertheless, both λ_{shear} and λ_{ext} show a dependence on the polymer concentration in the

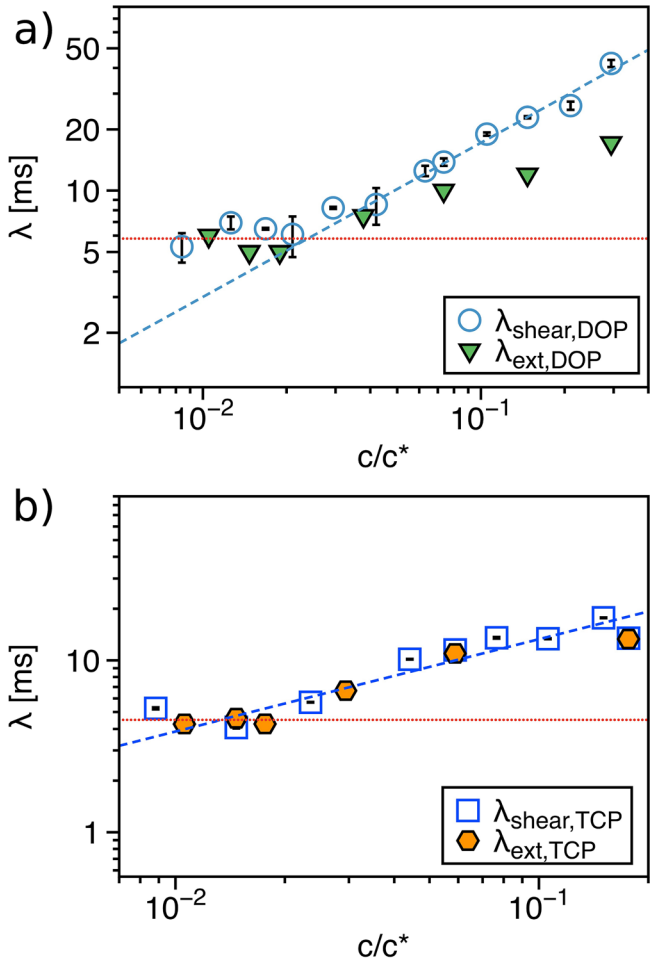

FIG. 4. (a) Relaxation time λ for a-PS in DOP as a function of the reduced concentration c/c^*. Note that $c^*_{DOP} = 0.54$ wt. %. Green triangles refer to the relaxation time measured through OSCER, λ_{ext}. Open blue circles refer to those measured through the μ-rheometer, λ_{shear}. The blue dashed line represents the best power law fit, $\lambda \propto c^{0.76\pm0.03}$. The red dotted line represents $\lambda_{0,DOP} = 5.8$ ms, obtained through an average of all the experimental data for $0.008 < c/c^* < 0.02$. The Zimm relaxation time from Eq. (2) for this system is $\lambda_{Zimm} = 14$ ms. (b) Relaxation time λ for a-PS in TCP as a function of the reduced concentration c/c^*. Note that $c^*_{TCP} = 0.2$ wt. %. Orange hexagons refer to the relaxation time measured through OSCER, λ_{ext}. Open blue squares refer to those measured through the μ-rheometer, λ_{shear}. The blue dashed line represents the best power law fit, $\lambda \propto c^{0.54\pm0.07}$. The red dotted line represents $\lambda_{0,DOP} = 4.2$ ms, obtained through an average of all the experimental data for $0.008 < c/c^* < 0.02$. The Zimm relaxation time from Eq. (2) for this system is $\lambda_{Zimm} = 54$ ms.

range $0.02 < c/c^* < 0.1$ [a blue dashed line in Fig. 4(a)], even if $c/c^* < 1$. Similar findings on both shear and extensional measures have been found by Clasen *et al.* [57]. In fact, they also observed a dependence of the relaxation time on the concentration when $10^{-2} < c/c^* < 1$ (dilute regime) for polymers in good (diethylphtalate) and athermal solvents (oligomeric styrene). Such a dependence is attributed to the increasing importance of intermolecular interactions when c approaches to c^*. Common methodologies to derive c^* are based on the assumption that overlap between two adjacent coils occurs when the distance between their centers of mass is equal to $2R_g$. For an extensional flow, it is fairly easy to understand that significant macromolecular deformation will result in an effective increase in R_g and hence promote interactions between chain ends for polymer concentrations $c < c^*$, as shown by Clasen *et al.* and others [57,61]. However, Odell *et al.* [61,62] have shown that even under equilibrium conditions, polymer chains may interact at concentrations significantly below c^*. They argue that the solid sphere model used to define c^* depends upon a poor approximation to a statistical random walk and show clearly that the Gaussian distribution of coil segments extend much further than R_g, away from the center of mass of the coil. Based on these considerations, we argue that in the vicinity of c^* the polymer dynamics can be described by the Rouse theory [Eq. (3)] instead of the Zimm theory [Eq. (2)], in agreement with the approach followed by Clasen *et al.* [57].

The data in Fig. 4(a) can be described by two scalings (blue dashed and red dotted lines). The blue dashed line shows a power law dependence of λ on c over the concentration interval $0.02 < c/c^* < 0.3$. We obtain a scaling $\lambda \propto c^{0.76\pm0.03}$ over this concentration range. We can use the exponent of 0.76 to obtain the value of the dimensionless scaling exponent $\nu = 0.52$ from Eq. (3) (Rouse theory), in very good agreement with the theory for polymer in theta-solvent ($\nu = 0.5$). The small discrepancy between our value of ν and the theoretical one can be possibly attributed to the lack of precise temperature control and some degree of polymer chain swelling since the experiments are performed approximately 3 °C above the theta temperature [24].

For $c/c^* < 0.02$, experimental data shown in Fig. 4(a) approach a constant value that is in agreement with the Zimm theory [3]. The red dashed line is obtained as the average of both λ_{shear} and λ_{ext} when $c/c^* < 0.02$, with an average relaxation time $\lambda_{0,DOP} = 5.8 \pm 0.75$ ms. We can then compare this value with λ_{Zimm} derived from Eq. (2). In particular, $F = 0.417$ (for $\nu = 0.52$) and the intrinsic viscosity $[\eta] = 2.1$ dl/g can be evaluated through the Mark-Houwink relation with the parameters available from the Polymer Handbook [58]. We then found $\lambda_{Zimm} \simeq 14$ ms, in reasonable agreement with $\lambda_{0,DOP}$ derived from our measurements.

Figure 4(b) shows the comparison between the relaxation time of polystyrene in TCP, derived through the μ-rheometer (blue open square) and those derived from the OSCER (orange hexagon). Both the microfluidic platforms are able to measure the relaxation time as small as 5 ms, and values of λ_{shear} and λ_{ext} are in good agreement. In this case, all the experimental data can be described by a single scaling $\lambda \propto c^{0.54\pm0.07}$ (by carrying out the same procedure adopted for a-PS in DOP). The value of the dimensionless scaling exponent is then $\nu = 0.55$, in good agreement with expectations for a polymer in a relatively good solvent [63].

Even though we do not observe a clear plateau region in Fig. 4(b), we can evaluate $\lambda_{0,TCP}$ as the average of the λ-values when $c/c^* < 0.02$. We found $\lambda_{0,TCP} = 4 \pm 2$ ms. The Zimm relaxation time derived from Eq. (2) with $F = 0.455$ (for $\nu = 0.55$), $[\eta] = 5$ dl/g, $\eta_s = 0.072$ Pa s, yields $\lambda_{Zimm} = 54$ ms, significantly higher than our estimate of $\lambda_{0,TCP}$. This is not surprising because the Zimm theory does not always match the experimental measurements for polymers in a good solvent [36,64]. Hair and Amis [64] carried out frequency response measurements on both polystyrene in theta and good solvents. They found good agreement between theory and experiments for the theta-

solvent only. The authors argue that a theory that consistently includes both hydrodynamic interactions and excluded volume would improve the agreement between experiments and the theory. Moreover, Lodge *et al.* [65] reported that the radius of gyration R_g of perdeuterated polystyrene in TCP, measured through small angle neutron scattering, is close to the values found for polystyrene in $\theta-$ solvent, thus being smaller than the one predicted through intrinsic viscosity measures. Our results seem to be consistent with this observation; in fact, the experimental relaxation time $\lambda_{0,TCP}$ is much smaller than λ evaluated from intrinsic viscosity measures by Eq. (2). The same authors attributed this discrepancy to the excluded volume for polymers in a good solvent. In particular, interactions between phenyl groups on the polystyrene and the solvents can lead to extra contributions to the viscosity. Such complexity motivated Colby [36] to classify the study of polymer in good solvents as an *outstanding problem left to be resolved* for polymer solutions.

Here, we highlight the agreement found between relaxation times derived in shear and extensional flows for a-PS in near-theta and a good solvent. Clasen *et al.* [57] measured the relaxation time of polystyrene in near-theta conditions by CaBER (extensional) and oscillatory shear measurements, showing large deviations between the two techniques above $c/c^* \sim 0.01$. Vadillo *et al.* [31] also reported disagreement between λ_{shear} derived from the piezo-axial vibrator (PAV) and λ_{ext} derived from capillary thinning extensional rheometry, for polystyrene in a good solvent. The techniques used by Clasen *et al.* and by Vadillo *et al.* for the determination of the relaxation time are based on bulk rheology. In our case, the μ-rheometer and the OSCER capture the local rheology at the microfluidic scale, and the agreement between λ_{shear} and λ_{ext} is ascribed to the working principle of these microfluidic platforms. The μ-rheometer is based on the balance between the elastic force (which promote the transversal migration) and the drag force. The elastic force is modeled from the second order fluid constitutive equation, with a single (longest) fluid relaxation time scaling linearly with the Deborah number *De* [21,45]. Such relaxation time, in the absence of intermolecular interactions, coincides with the Zimm relaxation time. With OSCER, the birefringence signal is observed when polymer molecules start to orient along the flow direction. The relaxation time measured in this configuration represents the longest relaxation time of the polymer chain, i.e., the Zimm relaxation time, with intrachain hydrodynamic interactions present in the case of the theta solvent, and partially screened hydrodynamic interactions in the case of the good solvent. Both the μ-rheometer and the OSCER, in the absence of intermolecular interactions, measure the Zimm relaxation time directly, thus explaining the agreement found between λ_{shear} and λ_{ext} when $c/c^* < 0.1$.

B. Polyelectrolytes in good solvent

1. Bulk shear rheology

The behavior of polyelectrolytes has been found distinctly different from that of neutral polymers [36,39], because of active charges on the polyelectrolyte chains. These charges can be screened by tuning the amount of salt in the solution, leading to molecular conformation changes of the polyelectrolyte [39,66,67]. In a salt-free environment and in the dilute polymer regime, polyelectrolytes tend to adopt an extended configuration due to the electrostatic interactions between free charges. With the addition of salt, counterions screen the charges, thus reducing electrostatic interactions, consequently altering the conformation from extended to random coils. In addition, the change of conformation in dilute polymer solutions occurs gradually, from the dilute salt regime to the concentrated salt regime. Here, we focus on rheological characterizations of hyaluronic acid (HA) in water, with the presence of organic salt sodium chloride (NaCl) at different concentrations.

First, we mixed HA at different mass concentrations in a PBS solution. PBS is routinely used as a suspending medium for cells and other biological samples and consists mainly of 138 mM NaCl and 2.7 mM of KCl [37,43]. Figure 5(a) shows the shear viscosity η as a function of the shear rate $\dot{\gamma}$ for HA in PBS solutions, with HA mass concentrations varying

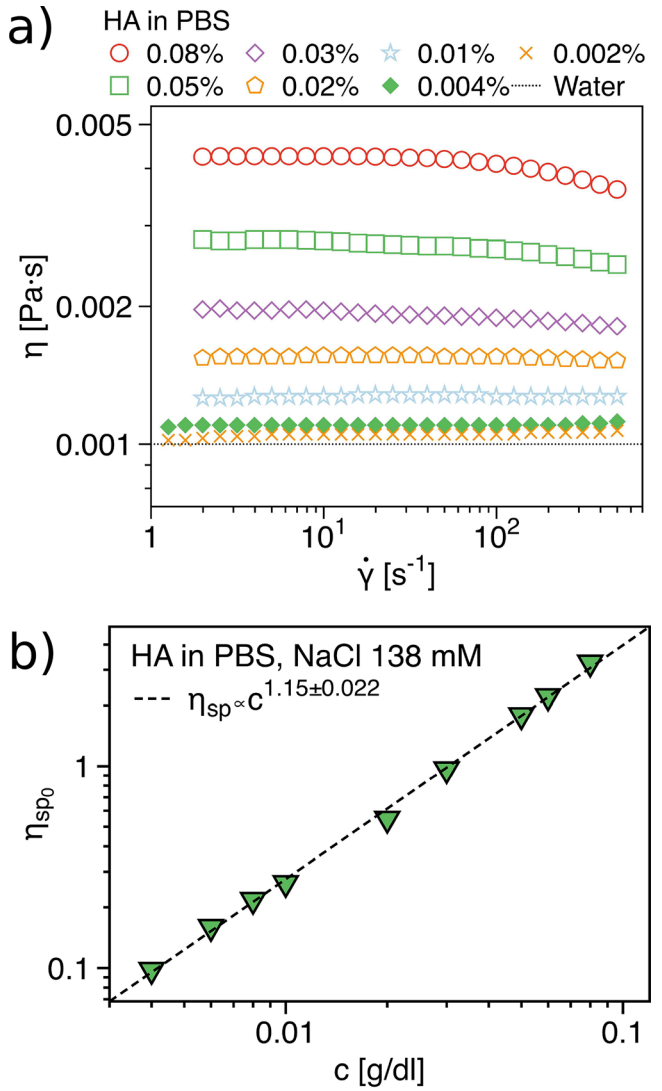

FIG. 5. (a) Shear viscosity η as a function of the shear rate $\dot{\gamma}$ for solutions at different concentrations of hyaluronic acid 1.6 MDa in PBS at 22 °C (polyelectrolyte in good solvent). (b) Specific viscosity as a function of the polymer concentration c for HA in PBS. The dashed line is a power-law best fit on the whole data set.

from 0.002 wt. % to 0.08 wt. %. All solutions exhibit near constant-viscosity in the shear rates $1 < \dot{\gamma} < 500\,s^{-1}$. To identify the dilute polymer regime, we plot the specific viscosity as a function of the polymer concentration c. The best power-law curve fit renders $\eta_{sp0} \propto c^{1.15\pm0.022}$ [see Fig. 5(b)], in agreement with the scaling relation reported by Krause *et al.* [37]. This dependence of η_{sp0} with the concentration is reported for dilute polyelectrolyte solutions in the high salt regime [39]. We can also estimate the overlapping concentration c^*, when $c^*[\eta] = 1.5$ (based on the work of Krause *et al.* [37]), with $[\eta] = 25$ dl/g [derived from the data of Fig. 5(b)]. We then obtain $c^* = 0.06$ g/dl in quantitative agreement with the result of Krause *et al.* [37]. We performed the same analysis of HA in water with 50 mM of NaCl and 100 mM of NaCl (data not shown). The rheological behavior of those solutions displays a similar trend of HA in PBS solutions, thus indicating that the amount of salt has saturated the free charges on the chain. In addition, the PBS solution contains 138 mM of NaCl, which is not far from the other salt solutions considered. We found $[\eta]_{50\,mM} \sim 32$ dl/g and $[\eta]_{100\,mM} \sim 26$ dl/g. The overlapping concentrations found for those systems are $c^*_{50\,mM} = 0.047$ g/dl and $c^*_{100\,mM} = 0.057$ g/dl.

2. Microfluidic approach

Figure 6 shows the relaxation time λ_{shear} as a function of the reduced concentration c/c^* for HA in water, with different NaCl concentrations. The measurement of λ_{ext} is not carried out due to the low birefringence of the HA solutions at these small concentrations. Moreover, we have found that with low viscosity solvents, measurements in the OSCER device can be complicated by the onset of inertial instabilities at the high strain rates required to achieve orientation in polymer samples with such short relaxation times [20,68]. By focusing on the data of λ_{shear} for HA in water with PBS (open blue diamonds), the relaxation time increases with increasing HA concentrations in the range of $0.04 < c/c^* < 1$, thus suggesting the existence of intermolecular interactions, as for a-PS in both near-theta and good solvents. By assuming a power law dependence [as suggested by Eq. (3)], we found $\lambda_{shear} \propto c^{1.00\pm0.036}$, with a power law index higher than the theoretical prediction for interacting not entangled chains $\lambda \propto c^{1/4}$ [37]. Krause *et al.* [37] performed relaxation time measurements on HA (with the same molecular weight used here) in PBS at several concentrations, all higher than those presented here.

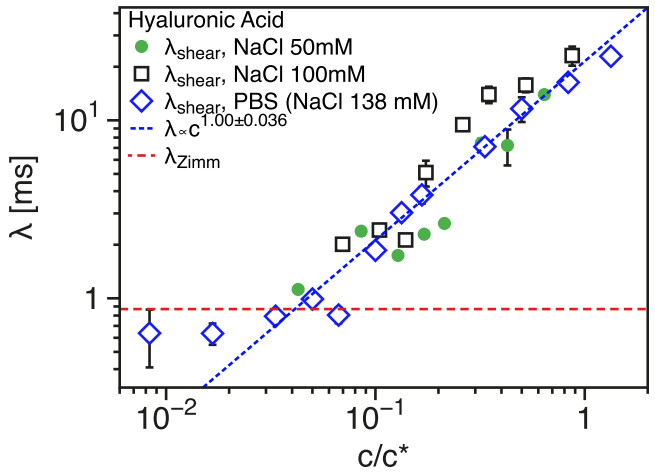

FIG. 6. Relaxation time λ for HA solution in water as a function of the reduced concentration c/c^*. Open blue diamonds refer to the relaxation time measured through the μ-rheometer, λ_{shear} for HA in water with the addition of PBS. Green circles and open squares are the measure of λ_{shear} for HA in water with 50 mM of NaCl and 100 mM of NaCl, respectively. The blue dashed line is the best fit on the blue diamonds for $c/c^* > 0.03$. We found $\lambda_{shear} \propto c$. The red dashed line is the relaxation time λ_{Zimm} from Zimm formula in Eq. (2).

In [37], the semidilute *entangled* regime was studied, and experimental data showed a polymer concentration dependence stronger than that expected from theory. Our data suggest that strong intramolecular interactions occur even at lower concentrations, and thus other parameters need to be considered in the model for the dynamics of polyelectrolyte solutions. Moreover, hyaluronic acid has been reported to be a very complex macromolecule [69–71] due to intrachain interactions, thus the comparison with the theoretical predictions can lead to results different from those expected.

Below a critical value $c/c^* \sim 0.04$, the relaxation time λ_{shear} is independent of the polymer concentration, as predicted by the Zimm theory when $c/c^* < 1$ [3] for neutral polymers in the dilute polymer regime, and by Dobrynin *et al.* [39]. An estimate of the relaxation time from the Zimm formula [3] gives $\lambda_{Zimm} \sim 0.87$ ms (red dashed line in Fig. 6), in very good agreement with our data for $c/c^* < 0.04$. By examining all the data of λ_{shear} for HA in water with 50 mM and 100 mM of NaCl, we notice that all the data follow the scaling $\lambda \propto c$, thus confirming that we are exploring the high salt regime. Indeed, at sufficiently high salt concentrations, the rheology of polyelectrolyte solutions is almost insensitive to the salt content [39].

V. CONCLUSIONS

In this work, we compare two microfluidic platforms, one based on shear flow (μ-rheometer) and another on extensional flows (OSCER), for the measurement of relaxation times down to milliseconds. These platforms have been used on different weakly viscoelastic fluids: (i) a neutral polymer in both theta and good solvents and (ii) polyelectrolyte in a good solvent with the presence of salt.

We summarize the following findings: (i) microfluidic techniques can capture very small relaxation times of dilute polymer solutions, not easily detectable by conventional rheometry techniques. (ii) λ_{shear} measured with the μ-rheometer is in very good agreement with λ_{ext} measured with the OSCER, for a-PS in both DOP and TCP. (iii) λ_{shear} and λ_{ext} show a dependence on c/c^* even in the dilute solution regime, suggesting that intermolecular interactions play a significant role at polymer concentrations below c^*. (iv) Our results on a-PS in the near-theta solvent DOP are well described by the Rouse model and, at the lowest concentrations explored, the relaxation time collapses to a plateau value that is in order-of-magnitude agreement with λ_{Zimm} [Eq. (2)]. (v) Our results on a-PS in a good solvent are in rather good agreement with the

Rouse theory. However, the predicted relaxation time λ_{Zimm} is much higher than our measured estimate, probably due to excluded volume effects, as reported in other works [36,64,65].

For polyelectrolyte solutions, only λ_{shear} is measured due to the low birefringence of the hyaluronic acid solutions. We found (i) a dependence of λ_{shear} with the polymer concentration, in agreement with our previous observations with a-PS in near-theta and good solvents. (ii) The scaling of λ_{shear} with the concentration cannot simply be explained in terms of intermolecular interactions as predicted by Rouse [2]. In addition, our exponent is also higher than those predicted by Dobrynin *et al*. [39] for polyelectrolyte in a semidilute unentangled polymer-regime in the presence of high salt amount. This discrepancy is not new in the literature, and can be ascribed to the complex nature of the hyaluronic acid [69–71]. (iii) When $c/c^* < 0.04$, λ_{shear} is in very good agreement with the relaxation time λ derived from the Zimm formula [3] (as predicted by Dobrynin *et al*. [39]).

We remark that for all the investigated polymer classes, the relaxation time is independent of the polymer concentration (as predicted by the Zimm theory [3]) only when $c/c^* \lesssim 0.02$, in agreement with the finding of Clasen *et al*. [57] for polystyrene in theta and good solvents. Even if polymer concentrations are below c^*, interactions between polymer chains take place. Our measurements then suggest that the "real" dilute regime, i.e., where polymer chains in a solution do not interact with each other, is recovered well below the overlapping concentration c^*.

Future works include investigation of even more dilute polymer solutions (i.e., $c/c^* < 0.01$) with smaller molecular weight, by using microfluidic techniques. We aim to show that microrheometrical techniques can provide a unique platform for the study of "ultra-dilute" polymer solutions.

References

[1] Alfrey, T., and P. Doty, "Statistical thermodynamics of high-polymer solutions I. Theory for dilute solutions," J. Chem. Phys. **13**, 77–83 (1945).

[2] Rouse, P. E., "A theory of the linear viscoelastic properties of dilute solutions of coiling polymers," J. Chem. Phys. **21**, 1272–1280 (1953).

[3] Zimm, B. H., "Dynamics of polymer molecules in dilute solution: viscoelasticity flow birefringence and dielectric loss," J. Chem. Phys. **24**, 269–278 (1956).

[4] Larson, R. G., "The rheology of dilute solutions of flexible polymers: Progress and problems," J. Rheol. **49**, 1–70 (2005).

[5] White, C. M., and M. G. Mungal, "Mechanics and prediction of turbulent drag reduction with polymer additives," Annu. Rev. Fluid Mech. **40**, 235–256 (2008).

[6] Rehage, H., and H. Hoffmann, "Viscoelastic surfactant solutions: Model systems for rheological research," Mol. Phys. **74**, 933–973 (1991).

[7] Discher, D. E., "Polymer vesicles," Science **297**, 967–973 (2002).

[8] Whitesides, G. M., "The origins and the future of microfluidics," Nature **442**, 368–373 (2006).

[9] D'Avino, G., and P. L. Maffettone, "Particle dynamics in viscoelastic liquids," J. Non-Newtonian Fluid **215**, 80–104 (2015).

[10] Del Giudice, F., G. D'Avino, F. Greco, P. A. Netti, and P. L. Maffettone, "Effect of fluid rheology on particle migration in a square-shaped microchannel," Microfluid. Nanofluid. **19**, 95–104 (2015).

[11] Zilz, J., R. J. Poole, M. A. Alves, D. Bartolo, B. Levaché, and A. Lindner, "Geometric scaling of a purely elastic flow instability in serpentine channels," J. Fluid Mech. **712**, 203–218 (2012).

[12] Pakdel, P., and G. H. McKinley, "Elastic instability and curved streamlines," Phys. Rev. Lett. **77**, 2459–2462 (1996).

[13] Lindner, A., "Flow of complex suspensions," Phys Fluid **26**, 101307 (2014).

[14] Rodd, L. E., J. J. Cooper-White, D. V. Boger, and G. H. McKinley, "Role of the elasticity number in the entry flow of dilute polymer solutions in micro-fabricated contraction geometries," J. Non-Newtonian Fluid **143**, 170–191 (2007).

[15] Nguyen, N.-T., Y.-C. Lam, S.-S. Ho, and C. L.-N. Low, "Improvement of rectification effects in diffuser/nozzle structures with viscoelastic fluids," Biomicrofluidics **2**, 034101 (2008).

[16] Farrell, C. J., A. Keller, M. J. Miles, and D. P. Pope, "Conformational relaxation time in polymer solutions by elongational flow experiments: 1. Determination of extensional relaxation time and its molecular weight dependence," Polymer **21**, 1292–1294 (1980).

[17] Carrington, S. P., and J. A. Odell, "How do polymers stretch in stagnation point extensional flow-fields?," J. Non-Newtonian Fluid **67**, 269–283 (1996).

[18] Miles, M. J., K. Tanaka, and A. Keller, "The behaviour of polyelectrolyte solutions in elongational flow; with the determination of conformational relaxation times (with an Appendix of an anomalous adsorption effect)," Polymer **24**, 1081–1088 (1983).

[19] Haward, S. J., M. S. N. Oliveira, M. A. Alves, and G. H. McKinley, "Optimized cross-slot flow geometry for microfluidic extensional rheometry," Phys. Rev. Lett. **109**, 128301 (2012).

[20] Haward, S. J., "Microfluidic extensional rheometry using stagnation point flow," Biomicrofluidics **10**, 043401 (2016).

[21] Macosko, C., *Rheology: Principles, Measurements, and Applications* (Wiley-VCH, New York, 1994).

[22] Pipe, C. J., T. S. Majmudar, and G. H. McKinley, "High shear rate viscometry," Rheol. Acta **47**, 621–642 (2008).

[23] Gupta, S., W. S. Wang, and S. A. Vanapalli, "Microfluidic viscometers for shear rheology of complex fluids and biofluids," Biomicrofluidics **10**, 043402 (2016).

[24] Colby, R. H., and M. Rubinstein, *Polymer Physics* (Oxford University, New York, 2003).

[25] Zilz, J., C. Schafer, C. Wagner, R. J. Poole, M. A. Alves, and A. Lindner, "Serpentine channels: Micro-rheometers for fluid relaxation times," Lab Chip **14**, 351–358 (2014).

[26] Del Giudice, F., G. D'Avino, F. Greco, I. D. Santo, P. A. Netti, and P. L. Maffettone, "Rheometry-on-a- chip: Measuring the relaxation time of a viscoelastic liquid through particle migration in microchannel flows," Lab Chip **15**, 783–792 (2015).

[27] Pipe, C. J., and G. H. McKinley, "Microfluidic rheometry," Mech. Res. Commun. **36**, 110–120 (2009).

[28] Del Giudice, F., V. Clacagno, V. E. Taliento, F. Greco, P. A. Netti, and P. L. Maffettone, "Relaxation time of polyelectrolyte solutions: when μ-rheometry steps in charge," J. Rheol. **61**(1), 13–21 (2017).

[29] Odell, J. A., and S. P. Carrington, "Extensional flow oscillatory rheometry," J. Non-Newtonian Fluid **137**, 110–120 (2006).

[30] Campo-Dean, L., and C. Clasen, "The slow retraction method (srm) for the determination of ultra-short relaxation times in capillary breakup extensional rheometry experiments," J. Non-Newtonian Fluid **165**, 1688–1699 (2010).

[31] Vadillo, D. C., W. Mathues, and C. Clasen, "Microsecond relaxation processes in shear and extensional flows of weakly elastic polymer solutions," Rheol. Acta **51**, 755–769 (2012).

[32] Keshavarz, B., V. Sharma, E. C. Houze, M. R. Koerner, J. R. Moore, P. M. Cotts, P. Threlfall-Holmes, and G. H. McKinley, "Studying the effects of elongational properties on atomization of weakly viscoelastic solutions using Rayleigh ohnesorge jetting extensional rheometry (rojer)," J. Non-Newtonian Fluid **222**, 171–189 (2015).

[33] Dinic, J., Y. Zhang, L. N. Jimenez, and V. Sharma, "Extensional relaxation times of dilute, aqueous polymer solutions," ACS Macro Lett. **4**, 804–808 (2015).

[34] Sousa, P. C., E. J. Vega, R. G. Sousa, J. M. Montanero, and M. A. Alves, "Measurement of relaxation times in extensional flow of weakly viscoelastic polymer solutions," Rheol. Acta **56**, 11–20 (2017).

[35] Bhattacharjee, P. K., A. G. McDonnell, R. Prabhakar, L. Y. Yeo, and J. Friend, "Extensional flow of low-viscosity fluids in capillary bridges formed by pulsed surface acoustic wave jetting," New J. Phys. **13**, 023005 (2011).

[36] Colby, R. H., "Structure and linear viscoelasticity of flexible polymer solutions: comparison of polyelectrolyte and neutral polymer solutions," Rheol. Acta **49**, 425–442 (2010).

[37] Krause, W. E., E. G. Bellomo, and R. H. Colby, "Rheology of sodium hyaluronate under physiological conditions," Biomacromolecules **2**, 65–69 (2001).

[38] Pfeuty, P., "Conformation des polyelectrolytes ordre dans les solutions de polyelectrolytes," J. Phys. Colloques **39**, C2–C149 (1978).

[39] Dobrynin, A. V., R. H. Colby, and M. Rubinstein, "Scaling theory of polyelectrolyte solutions," Macromolecules **28**, 1859–1871 (1995).

[40] Berry, G. C., "Thermodynamic and conformational properties of polystyrene. ii. intrinsic viscosity studies on dilute solutions of linear polystyrenes," J. Chem. Phys. **46**, 1338–1352 (1967).

[41] Hua, C. C., and M. S. Wu, "Viscometric properties of dilute polystyrene/dioctyl phthalate solutions," J. Polym. Sci. B. Polym. Phys. **44**, 787–794 (2006).

[42] Riande, E., H. Markovitz, D. J. Plazek, and N. Raghupathi, "Viscoelastic behavior of polystyrene-tricresyl phosphate solutions," J. Polym. Sci. C. Polym. Symp. **50**, 405–430 (2007).

[43] Lim, E. J., T. J. Ober, J. F. Edd, S. P. Desai, D. Neal, K. W. Bong, P. S. Doyle, G. H. McKinley, and M. Toner, "Inertio-elastic focusing of bioparticles in microchannels at high throughput," Nat. Commun. **5**, 4120 (2014).

[44] Leshansky, A. M., A. Bransky, N. Korin, and U. Dinnar, "Tunable nonlinear viscoelastic 'focusing' in a microfluidic device," Phys. Rev. Lett. **98**, 234501 (2007).

[45] Romeo, G., G. D'Avino, F. Greco, P. A. Netti, and P. L. Maffettone, "Viscoelastic flow-focusing in microchannels: Scaling properties of the particle radial distributions," Lab Chip **13**, 2802–2807 (2013).

[46] Haward, S. J., A. Jaishankar, M. S. N. Oliveira, M. A. Alves, and G. H. McKinley, "Extensional flow of hyaluronic acid solutions in an optimized microfluidic cross-slot device," Biomicrofluidics **7**, 044108 (2013).

[47] Adam, N., and P. Ghosh, "Hyaluronan molecular weight and polydispersity in some commercial intra-articular injectable preparations and in synovial fluid," Inflamm. Res. **50**, 294–299 (2001).

[48] Maleki, A., A.-L. Kjpniksen, and B. Nystrom, "Anomalous viscosity behavior in aqueous solutions of hyaluronic acid," Polym. Bull. **59**, 217–226 (2007).

[49] de Gennes, P. G., "Coil-stretch transition of dilute flexible polymers under ultrahigh velocity gradients," J. Chem. Phys. **60**, 5030–5042 (1974).

[50] Perkins, T. T., "Single polymer dynamics in an elongational flow," Science **276**, 2016–2021 (1997).

[51] Hinch, E. J., "Mechanical models of dilute polymer solutions in strong flows," Phys. Fluid **20**, S22–S30 (1977).

[52] Larson, R. G., and J. J. Magda, "Coil-stretch transitions in mixed shear and extensional flows of dilute polymer solutions," Macromolecules **22**, 3004–3010 (1989).

[53] Keller, A., and J. A. Odell, "The extensibility of macromolecules in solution: A new focus for macromolecular science," Colloid Polym. Sci. **263**, 181–201 (1985).

[54] Haward, S. J., "Characterization of hyaluronic acid and synovial fluid in stagnation point elongational flow," Biopolymers **101**, 287–305 (2014).

[55] Han, C.-Y., and Y.-F. Chao, "Photoelastic modulated imaging ellipsometry by stroboscopic illumination technique," Rev. Sci. Instrum. **77**, 023107 (2006).

[56] Nichols, S., J. Freudenthal, O. Arteaga, and B. Kahr, "Imaging with photoelastic modulators," Proc. SPIE **9099**, 909912 (2014).

[57] Clasen, C., J. P. Plog, W.-M. Kulicke, M. Owens, C. Macosko, L. E. Scriven, M. Verani, and G. H. McKinley, "How dilute are dilute solutions in extensional flows?," J. Rheol. **50**, 849–881 (2006).

[58] Brandrup, J., E. H. Immergut, E. A. Grulke, A. Abe, and B. R. Bloch, *Polymer Handbook* (Wiley, New York, 1989), Vol. 7.

[59] de Gennes, P. G., and T. A. Witten, "Scaling concepts in polymer physics," Phys. Today **33**(6), 51 (1980).

[60] Osaki, K., T. Inoue, and T. Uematsu, "Stress overshoot of polymer solutions at high rates of shear: Semidilute polystyrene solutions with and without chain entanglement," J. Polym. Sci. B. Polym. Phys. **38**, 3271–3276 (2000).

[61] Odell, J. A., A. Keller, and M. J. Miles, "Assessment of molecular connectedness in semi-dilute polymer solutions by elongational flow," Polymer **26**, 1219–1226 (1985).

[62] Odell, J., A. Keller, and A. Muller, "Extensional flow behavior of macromolecules in solution," in *Polymers in Aqueous Media: Performance through Association* (American Chemical Society, Washington DC, 1989), pp. 193–244.

[63] Tirtaatmadja, V., G. H. McKinley, and J. J. Cooper- White, "Drop formation and breakup of low viscosity elastic fluids: Effects of molecular weight and concentration," Phys. Fluids **18**, 043101 (2006).

[64] Hair, D. W., and E. J. Amis, "Intrinsic dynamic viscoelasticity of polystyrene in. theta. and good solvents," Macromolecules **22**, 4528–4536 (1989).

[65] Lodge, T. P., K. C. Hermann, and M. R. Landry, "Coil dimensions of polystyrenes in isorefractive viscous solvents by small-angle neutron scattering," Macromolecules **19**, 1996–2002 (1986).

[66] Dobrynin, A. V., and M. Rubinstein, "Theory of polyelectrolytes in solutions and at surfaces," Prog. Polym. Sci. **30**, 1049–1118 (2005).

[67] Buhler, E., and F. Boue, "Chain persistence length and structure in hyaluronan solutions: Ionic strength dependence for a model semirigid polyelectrolyte," Macromolecules **37**, 1600–1610 (2004).

[68] Haward, S. J., and G. H. McKiney, "Instabilities in stagnation point flows of polymer solutions," Phys. Fluids **25**, 083104 (2013).

[69] Dubrovskii, S. A., A. N. Zelenetskii, S. A. Uspenskii, and V. N. Khabarov, "Effect of borax additives on the rheological properties of sodium hyaluronate aqueous solutions," Polym. Sci. Ser. A **56**, 205–210 (2014).

[70] Fouissac, E., M. Milas, and M. Rinaudo, "Shear-rate, concentration, molecular weight, and temperature viscosity dependences of hyaluronate, a wormlike polyelectrolyte," Macromolecules **26**, 6945–6951 (1993).

[71] Morris, E. R., D. A. Rees, and E. J. Welsh, "Conformation and dynamic interactions in hyaluronate solutions," J. Mol. Biol. **138**, 383–400 (1980).